Accelerated Article Preview

Single Molecule Infrared Spectroscopy in the Gas Phase

Received: 9 December 2022

Accepted: 21 June 2023

Accelerated Article Preview

Cite this article as: Calvin, A. et al. Single Molecule Infrared Spectroscopy in the Gas Phase. *Nature* https://doi.org/10.1038/ s41586-023-06351-7 (2023) Aaron Calvin, Scott Eierman, Zeyun Peng, Merrell Brzeczek, Lincoln Satterthwaite & David Patterson

This is a PDF file of a peer-reviewed paper that has been accepted for publication. Although unedited, the content has been subjected to preliminary formatting. Nature is providing this early version of the typeset paper as a service to our authors and readers. The text and figures will undergo copyediting and a proof review before the paper is published in its final form. Please note that during the production process errors may be discovered which could affect the content, and all legal disclaimers apply.

Single Molecule Infrared Spectroscopy in the Gas Phase

Aaron Calvin, Scott Eierman, Zeyun Peng, Merrell Brzeczek, Lincoln Satterthwaite, and David Patterson

1) Department of Physics, University of California, Santa Barbara

(*Electronic mail: davepatterson@ucsb.edu)

Spectroscopy is a key analytical tool that provides valuable insight into molecular structure and is widely used to identify chemical samples. Tagging spectroscopy is a form of action spectroscopy in which the absorption of a single photon by a molecular ion is detected via the loss of a weakly attached, inert "tag" particle (e.g. He, Ne, N_2). ¹⁻³ The absorption spectrum is derived from the tag loss rate as a function of incident radiation frequency. To date, all spectroscopy of gas phase polyatomic molecules has been restricted to large molecular ensembles, complicating spectral interpretation by the presence of multiple chemical and isomeric species. Here we present a novel tagging spectroscopic scheme to analyze the purest possible sample: a single gas phase molecule. We demonstrate this technique with the measurement of the infrared spectrum of a single tropylium $(C_7H_7^+)$ molecular ion; to our knowledge the first recorded spectrum of a single gas phase polyatomic molecule. Our method's high sensitivity revealed spectral features previously unobserved using traditional tagging methods. Our approach in principle enables analysis of multi-component mixtures by identifying constituent molecules one at a time. Single molecule sensitivity extends action spectroscopy to rare samples, such as those of extraterrestrial origin, 5,6 or to reactive reaction intermediates formed at number densities too low for traditional action methods.

Single molecule spectroscopy in the condensed phase has been a fruitful area of research for decades, ^{7,8} but distortions from interaction-induced effects are unavoidable in condensed phase spectra. Gas phase single molecule spectroscopy has so far been limited to photodissociation and quantum logic measurements of diatomic molecular ions. 9-12 Similar to our setup, these studies translationally cool a molecular ion to submillikelvin temperatures via the Coulomb interaction with a co-trapped, laser-cooled atomic ion partner. This sympathetic cooling process leaves the ions arranged in an ordered Coulomb crystal, where they are highly spatially localized and isolated from the environment. These features make lasercooled Coulomb crystals an ideal platform for multiple forms of spectroscopy, ^{13,14} where effectively indefinite trap lifetimes make even very weak transitions accessible. 15,16 Quantum logic techniques in particular remain the gold standard for high resolution single molecule measurements. In spite of this resolution advantage, however, these methods are often technically challenging to implement and difficult to apply to arbitrary molecular species. Quantum logic is therefore invaluable for fundamental physics and precision measurement experiments, 17,18 but impractical as a tool for chemical analysis. By adapting non-destructive mass spectrometry methods that are uniquely possible with laser-cooled Coulomb crystals, ¹⁹ we are able to record a spectrum via the detection

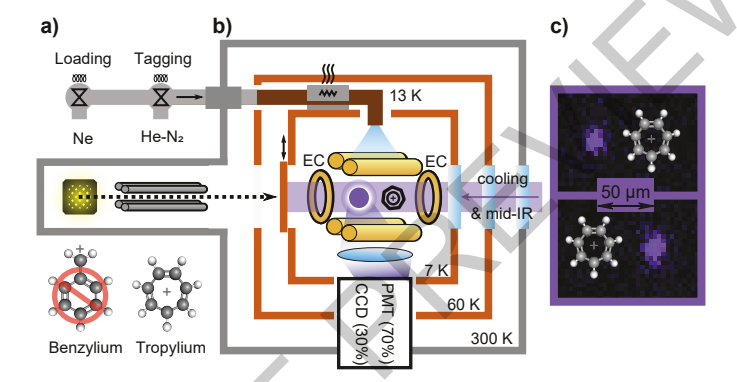


Figure 1: Single molecule tagging setup | a) Ions are produced at room temperature and mass filtered before trapping. The competing mass 91 Da isomer benzylium (Bz⁺) is formed along with Tr⁺, but only Tr⁺ is trapped due to the photodissociation of Bz⁺ by 422 nm laser light.²⁰ Neon is pulsed into the trapping region during loading to dissipate the kinetic energy of incoming ions via collisions. After loading, a mechanical shutter is closed to separate the cold experimental region from the room temperature ionization region. b) Trap details are discussed in the Methods. ⁸⁸Sr⁺ and Tr⁺ are co-trapped in a linear quadrupole trap with two endcap (EC) electrodes confining the ions along the trap axis. A 10:1 mixture of He:N₂ cooled to 13 K is pulsed into the trapping region, tagging the molecular ion with N₂. An AC voltage applied between the endcaps drives secular oscillation, which modulates the ⁸⁸Sr⁺ fluorescence. Lenses below the trap collect fluorescence light and image it onto a CCD camera and PMT. c) Two CCD images show ⁸⁸Sr⁺ and Tr⁺ flipping between two possible positions along the trap axis. Tr⁺ is dark to direct observation and is represented by a ball-and-stick model.

of tagging- de-tagging cycles. This approach is technically simple to implement and is generalizable to a broad class of polyatomic molecules.

Experimental

 $^{88}Sr^+$ is trapped in a linear Paul trap and Doppler cooled to millikelvin temperatures by driving the 5p $^2P_{1/2} \rightarrow 5s~^2S_{1/2}$ transition with red-detuned 422 nm laser light. About 6×10^3 scattered photons per second are collected and recorded by a CCD camera and a photomultiplier tube (PMT), with 70% going to the PMT for photon correlation measurements (see Fig. 1). A single molecular ion is mass-selected before being co-trapped with a single $^{88}Sr^+$ atomic ion, which sympathet-

²⁾Department of Chemistry and Biochemistry, University of California, Santa Barbara

ically cools the molecule to millikelvin translational temperatures via the ions' mutual Coulomb interaction. Like nearly all molecules, Tr⁺ lacks the level structure necessary for efficient laser cooling and rarely scatters photons from the 422 nm cooling light. Hence, the molecular ion is dark to direct observation.

The molecular ion's mass is determined non-destructively by observing the photons scattered by ⁸⁸Sr⁺. The Coulomb crystallized molecular ion-atomic ion pair forms a coupled oscillator confined within the trap's pseudo-harmonic potential, with a characteristic secular frequency which depends on the mass of both ions. We drive the ion pair to oscillate at the secular frequency, which modulates the ⁸⁸Sr⁺ fluorescence intensity at the same frequency via the Doppler effect. This modulation can be directly observed with a PMT (see Fig. 2a).

For the two ion Coulomb crystals that we study here, there is a simple analytical relationship between the ions' axial oscillation frequency and their total mass.²¹ The mass of the atomic ion is already known precisely, however, so that a measurement of the axial secular frequency of the crystal directly reveals the mass of the molecular ion. We employ a novel chirped voltage pulse method to initially measure the mixed Coulomb crystal's axial frequency, both with and without a tag attached to the molecule (See Methods). Once measured, we detect the presence and absence of tags by driving ion motion at the ⁸⁸Sr⁺-Tr⁺·N₂ resonant frequency. A lock-in amplifier compares the drive frequencies with the observed ⁸⁸Sr⁺ fluorescence modulation and outputs a signal proportional to the fluorescence correlation. This process is illustrated in Fig. 2. Changes in the molecule's tag state are therefore observed as discontinuous changes in the lock-in signal amplitude.

Nitrogen is our tag species of choice, as it readily tags most molecules and remains attached with a long lifetime, enabling us to observe weak transitions through slow de-tagging events. Molecular ions are tagged with N_2 using a 10:1 mixture of He: N_2 . Short pulses of this gas mixture flow through a cryogenic heat exchanger, which cools it to 13 K before it enters the trapping region. Helium efficiently removes kinetic energy from the system during ternary molecule-He- N_2 collisions, leaving N_2 weakly bound to the molecule. In the case of Tr^+ , the lifetime of this complex is several hours in the absence of mid-IR laser light. This leads to a near-zero background de-tagging rate on the timescale of our experiment, enabling us to observe very weak spectral features invisible to most other methods.

Molecules are de-tagged with mid-IR light from a commercial optical parametric oscillator (OPO). The OPO output has a spectral linewidth of 6 cm⁻¹ over the region of interest and is co-aligned with light from the cooling lasers along the axis of the ion trap. As shown in Fig. 2a, a Coulomb crystal with a single tagged Tr⁺ is driven to oscillate at its secular frequency by a sinusoidal voltage applied to a trap endcap electrode. This drive signal is sent to a lock-in amplifier, where it is compared to the fluorescence signal observed by the PMT. The frequencies of the two signals are initially equal, thus producing a high lock-in output signal. A sequence of mid-IR pulses of varying length are sent to the trap while the secular

motion is being driven. Resonant de-tagging of the molecule causes the secular frequency of the ions to jump discontinuously (Fig. 2b), eliminating the correlation between the applied drive voltage and the observed fluorescence modulation (Fig. 2c). The observed lock-in signal therefore drops to nearzero, indicating that a de-tagging event has occurred. The total duration of all mid-IR pulses up to the point of de-tagging is then recorded, providing a de-tagging time and corresponding rate. The molecular ion is then re-tagged for further measurements at different mid-IR laser frequencies. Near resonance, the mid-IR light de-tags molecular ions on a timescale of tens of milliseconds. Off resonance, no de-tagging events occur within 90 seconds, giving a baseline >90 seconds. This wide dynamic range makes weaker transitions with lifetimes of many seconds easily observable. The total time required to acquire a data point in a spectrum varies with the de-tagging time, but on the average it takes approximately two minutes to prepare a tagged molecule and subsequently de-tag it. While a molecule can be recycled for many tag-detag cycles, it is occasionally lost to reactions with background contaminants. Under favorable circumstances, as shown in figure 3a, we can obtain a spectrum from a single molecule, although in our followup work with other molecules, we typically found that between one and five molecules are needed to obtain a clear spectrum.²² While the data acquisition time for our method is much longer than in traditional tagging spectroscopy, the innate purity of our single molecule samples results in simpler observed spectra.

Single Molecule Spectrum

The vibrational spectrum of a single Tr⁺ molecule in the C-H stretching region is shown in Fig. 3a), spanning 2944–3150 cm⁻¹. This single molecule data is consistent with a composite spectrum taken from eight individual Tr⁺ ions, shown in Fig. 3b). A maximum likelihood estimate of the de-tagging time constant at every frequency step is calculated from the three de-tagging observations. The de-tagging rates reported in Fig. 3 are the inverse of these calculated time constants. The vertical bars in Fig. 3b) are 95% confidence intervals derived from the de-tagging probability distribution at each frequency step which is centered on the estimated most likely time constant. Single molecule measurements from eight total molecular ions were used for this averaged spectrum, as the molecules were occasionally lost from the trap. These losses are attributed to reactive collisions with residual background gases such as O_2 .

The dominant feature in this spectrum at 3042 cm⁻¹ is consistent with previous tagging experiments,⁴ which assigned this transition as the lone IR-active, asymmetric C–H stretching mode of Tr⁺. A single transition at 3074 cm⁻¹ was also reported, but the enhanced resolution of our method compared to conventional tagging spectroscopy allows us to resolve a previously unseen splitting of this peak into two features at 3065 and 3077 cm⁻¹. Multiple studies of Tr⁺ have observed this band,²³ but it has yet to be assigned. In addition to these primary peaks, we observe weak transitions at 2952 and 3140

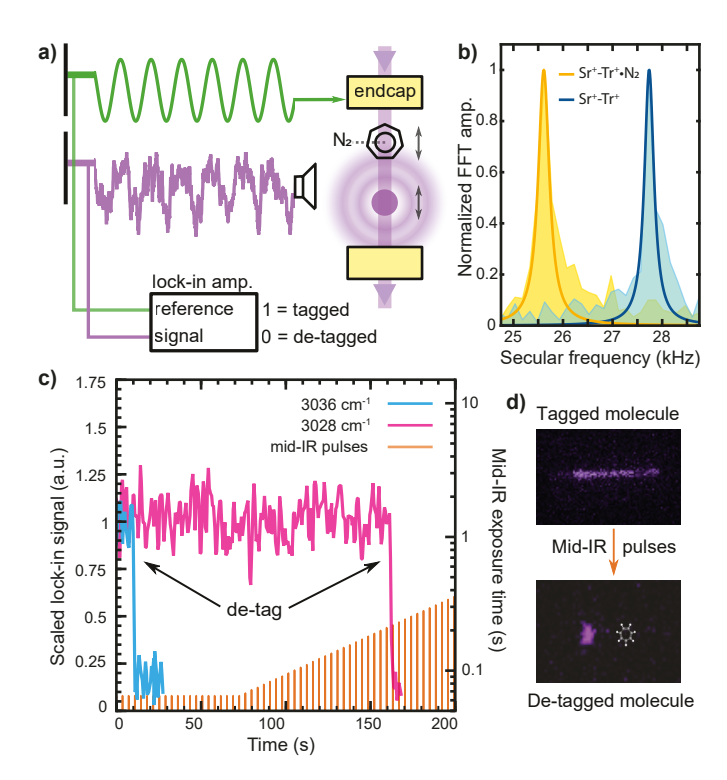


Figure 2: De-tagging detection | a) An AC drive voltage (green) is resonant with the ⁸⁸Sr⁺-Tr⁺·N₂ secular frequency, causing the ions to oscillate. The resulting Doppler modulation of the ⁸⁸Sr⁺ fluorescence intensity is observed by a PMT (purple). A lock-in amplifier compares the PMT signal with the AC drive, producing a near-unity voltage when the drive is resonant, and near-zero when not. b) The axial secular frequency of a 88 Sr⁺-Tr⁺ Coulomb crystal decreases by several kHz when Tr⁺ is tagged. The measurement in a) is done at these two frequencies, and the resulting lock-in signals indicate the tagged state of the molecule. c) A tagged molecule is exposed to a sequence of mid-IR light pulses. The pulses are initially of fixed length, later increasing exponentially in duration. Incident mid-IR photons drive vibrational transitions which remove the molecule's tag. This is observed as a discontinuous drop in the lock-in amplifier signal. Fast (blue) and slow (pink) de-tagging events are shown. When a de-tagging event is detected, the total exposure time from the mid-IR pulse train is summed and inverted to produce a de-tagging rate. d) CCD camera images of a Coulomb crystal with a tagged molecule driven to oscillate, which ceases oscillation after de-tagging.

cm⁻¹. These peaks lay below the noise floor of other action spectroscopy methods and have therefore not been reported previously. Theoretical work to aid in the detailed assignment of all four weak bands is ongoing, but these are likely attributable to weak combination or overtone transitions.

Although our method measures the absorption spectrum of the molecular ion-tag Van der Waals complex, such as $Tr^+\cdot N_2$, this spectrum is a very close analog to that of the bare molecular ion. Selection rules and transition frequencies are slightly perturbed by the presence of a tag, but typ-

ical line shifts are on the order of a few cm⁻¹.²⁴ Proposed¹⁵ and demonstrated²⁵ methods to study bare molecular ions are compatible with the single molecule technique demonstrated here and, in principal, could leverage the highly controlled environment of the Coulomb crystal to yield very high resolution, rotationally resolved single molecule spectra.

The linewidths observed for transitions in Fig. 3 are limited both by the spectral profile of our OPO light source, as well as the natural timescale for the de-tagging process. While this timescale is different for each molecule, it is predicted to range anywhere from 0.1-100 ps, 26 giving a natural frequency resolution limit on the order of 10 GHz - 10 THz. Our observed noise level is dominated by sampling error, which is proportional to the de-tagging rate and is reduced by repeated measurements. We find that three repetitions at each wavelength sampled are sufficient to reduce our sampling error to identify repeatable spectral features. Since the tagged lifetime for ${\rm Tr}^+ \cdot {\rm N}_2$ is several hours in the absence of mid-IR light, and >90 seconds off resonance, we are able to measure de-tagging events up to 90 seconds with a near-zero background.

Tr⁺ has been the subject of exhaustive study for over a century, largely owing to the long held belief that this unique aromatic cation contributes to the m = 91 Da component of alkylbenzene mass spectra. 27,28 Tagging spectroscopy has recently confirmed the presence of Tr⁺ in such fragmentation processes, 4,29 along with isomeric benzylium (Bz⁺, see Fig. 1). The two isomers often form at similar rates and thus both contribute to observed spectra, complicating the assignment process. While our single molecule technique is uniquely suited to distinguish between these competing isomers through sequential measurements, this process proves unnecessary in our system. Bz⁺ is known to readily dissociate when exposed to 422 nm light, ²⁰ which is necessarily present in our system for laser cooling. Tr⁺ is therefore the only mass 91 Da isomer that we observe, confirmed by the absence of known Bz⁺ transitions at 2997 or 3116 cm⁻¹ in our spectra.⁴ Additionally, any isomerization of trapped Tr⁺ to Bz⁺ would lead to rapid photodissociation and spontaneous loss of the molecule, which we do not observe. Bz⁺ studies could easily be realized with the choice of a different atomic species for laser cooling.

The perturbations caused by the Van der Waals adhered tag do not prevent identification of the molecular ion through the measurement of vibrational transitions. In general, the infrared absorption spectrum as measured here is insufficient to determine the structure of a previously unknown species, but is sufficient to distinguish different species and definitively identify a compound if its spectrum is previously known. Such identification could prove useful in the analysis of rare samples. For example, molecules from the moons of Saturn have been characterized in situ previously via mass spectrometry, ⁶ where organic molecular ions such as C₇H₇⁺ have been identified. Definitive identification of the structures of these molecules is beyond the state of the art for such tools, however, making an adaptation of our single molecule spectroscopic method an attractive alternative for such rare samples. Competing isomers of C₇H₇⁺ could be resolved given the library of spectra already obtained on the two

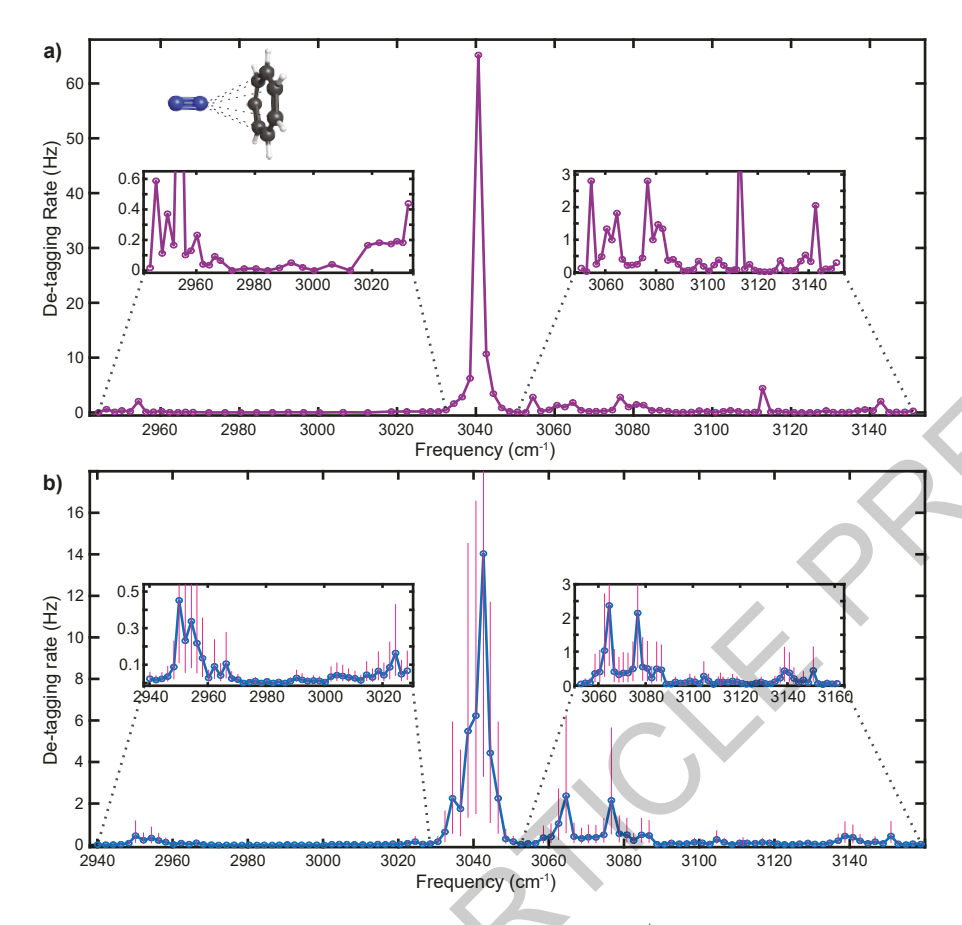


Figure 3: Single molecule spectrum | a) The infrared spectrum of a single Tr^+ molecule in the C-H stretching region. The strong transition at 3040 cm⁻¹ is consistent with previously reported values for N_2 -tagged Tr^+ , which assign this transition as an asymmetric C-H stretch. Weak transitions, invisible to most other action techniques, are shown in the insets. We broadly attribute these features to combination bands. b) A composite of eight single molecule measurements. Three de-tagging measurements were made every 2 cm⁻¹. Maximum likelihood estimates of the de-tagging time constant are calculated at each point as described in the Methods, with vertical bars indicating 95% confidence intervals for these values. The primary peak shifts slightly to 3042 cm⁻¹ with these additional measurements. The confidence interval on the primary peak extends to 39 Hz. A total of eight Tr^+ molecules were used to measure all plotted points, as molecules were periodically lost due to reactive collisions with background gas.

isomers. Extension to more complex mixtures would require a library of spectral data for the expected molecules at each mass. In principle, a mature version of our single molecule method would allow the deconvolution of complex mixtures with no confusion from overlapping spectra.

We also expect our single molecule method could find application in characterizing mixed-species products produced in cold and astrochemically relevant chemical reactions^{30,31} without the need for prior purification. Since our spectral measurement is non-destructive to the analyte molecule, the spectra could be used to identify both charged reactants and products. In this case, *ab initio* calculations would guide assignment by narrowing the list of likely reaction products based on energetics. Although measuring the C-H stretch as we have shown here could provide identification for sufficiently distinct candidate molecules, our method is easily extended to the fingerprint region (between 400 and 1500 cm⁻¹), where low energy C-H bending modes pro-

vide molecule-specific transitions. Experiments have been ongoing to demonstrate this technique on other molecular ion species and study the product distribution of a single molecule photofragmentation reaction.

¹Wolk, A.B., Leavitt, C.M., Garand, E., Johnson, M.A. Cryogenic ion chemistry and spectroscopy. Acc. Chem. Res. **47**(1), 202–210 (2013)

²Pereverzev, A., Roithová, J. Experimental techniques and terminology in gas-phase ion spectroscopy. J. Mass Spectrom. 57(5), 4826 (2022)

³Campbell, E.K., Holz, M., Gerlich, D., Maier, J.P. Laboratory confirmation of C_{60}^+ as the carrier of two diffuse interstellar bands. Nature **523**(7560), 322–323 (2015)

 4 Wagner, J.P., McDonald II, D.C., Duncan, M.A. Mid-infrared spectroscopy of $C_7H_7^+$ isomers in the gas phase: benzylium and tropylium. J. Phys. Chem. Lett. **9**(16), 4591–4595 (2018)

⁵Naraoka, H., *et al.*Soluble organic molecules in samples of the carbonaceous asteroid (162173) Ryugu. Science **379**, 9033 (2023)

⁶Waite Jr., J.H., *et al.*Cassini ion and neutral mass spectrometer: Enceladus plume composition and structure. Science **311**(5766), 1419–1422 (2006)

⁷Moerner, W.E., Kador, L. Optical detection and spectroscopy of single molecules in a solid. Phys. Rev. Lett. **62**(21), 2535–2538 (1989)

- ⁸Braeken, E., *et al*. Single molecule probing of the local segmental relaxation dynamics in polymer above the glass transition temperature. J. Am. Chem. Soc. **131**(34), 12201–12210 (2009)
- ⁹A. K. Hansen, M.A.S., Staanum, P.F., Drewsen, M. Single-ion recycling reactions. Angew. Chem. **51**, 7960–7962 (2012)
- ¹⁰Wolf, F., et al.Non-destructive state detection for quantum logic spectroscopy of molecular ions. Nature 530, 457–460 (2016)
- ¹¹Sinhal, M., Meir, Z., Najafian, K., Hegi, G., Willitsch, S. Quantum-nondemolition state detection and spectroscopy of single trapped molecules. Science 367(6483), 1213–1218 (2020)
- ¹²Sinhal, M., Willitsch, S. Molecular-Ion Quantum Technologies, pp. 305–332. John Wiley & Sons, Ltd, (2023). Chap. 13
- ¹³Calvin, A.T., Brown, K.R. Spectroscopy of molecular ions in Coulomb crystals. J. Phys. Chem. Lett. 9(19), 5797–5804 (2018)
- ¹⁴Willitsch, S. Coulomb-crystallised molecular ions in traps: methods, applications, prospects. Int. Rev. Phys. Chem. 31(2), 175–199 (2012)
- ¹⁵Khanyile, N.B., Shu, G., Brown, K.R. Observation of vibrational overtones by single-molecule resonant photodissociation. Nat. Commun. 6(1), 7825 (2015)
- ¹⁶Germann, M., Tong, X., Willitsch, S. Observation of electric-dipole-forbidden infrared transitions in cold molecular ions. Nat. Phys. 10(11), 820–824 (2014)
- ¹⁷Chou, C.-W., et al. Preparation and coherent manipulation of pure quantum states of a single molecular ion. Nature 545(7653), 203–207 (2017)
- ¹⁸ Alighanbari, S., Giri, G.S., Constantin, F.L., Korobov, V.I., Schiller, S. Precise test of quantum electrodynamics and determination of fundamental constants with HD⁺ ions. Nature 581(7807), 152–158 (2020)
- ¹⁹Sheridan, K., Keller, M. Weighing of trapped ion crystals and its applications. New J. Phys. 13(12), 123002 (2011)
- ²⁰Fèraud, G., Dedonder-Lardeux, C., Soorkia, S., Jouvet, C. Photo-fragmentation spectroscopy of benzylium and 1-phenylethyl cations. J. Chem. Phys. **140**, 024302 (2014)
- ²¹Morigi, G., Walther, H. Two-species Coulomb chains for quantum information. Eur. Phys. J. D 13, 261–269 (2001)
- ²²Eierman, S., et al. A cryogenic ion trap for single molecule vibrational spectroscopy. Rev. Sci. Instrum. Manuscript in press
- ²³Fateley, W.G., Lippincott, E.R. Vibrational spectrum and structure of the tropylium ion. J. Chem. Phys. 26(6), 1471–1481 (1957)
- ²⁴Johnson, C.J., et al. Communication: He-tagged vibrational spectra of the SarGlyH⁺ and H⁺(H₂O)_{2,3} ions: quantifying tag effects in cryogenic ion vibrational predissociation (CIVP) spectroscopy. J. Chem. Phys. **140**(22), 221101 (2014)
- ²⁵Schmid, P.C., Asvany, O., Salomon, T., Thorwirth, S., Schlemmer, S. Leakout spectroscopy, a universal method of action spectroscopy in cold ion traps. J. Phys. Chem. A **126**(43), 8111–8117 (2022)
- ²⁶Puttkamer, K., Dübal, H.R., Quack, M. Time-dependent processes in polyatomic molecules during and after intense infrared irradiation. Faraday Discuss. 75, 197–210 (1983)
- ²⁷Merling, G. Ueber tropin. Ber. or Chem. Ber. **24**(2), 3108–3126 (1891)
- ²⁸Rylander, P.N., Meyereson, S., Grubb, H.M. Organic ions in the gas phase. II. the tropylium ion. J. Am. Chem. Soc. 79(4), 842–846 (1957)
- ²⁹ Jusko, P., Simon, A., Banhatti, S., Brünken, S., Joblin, C. Direct evidence of the benzylium and tropylium cations as the two long-lived isomers of C₇H₇⁺. ChemPhysChem 19, 3182–3185 (2018)
- ³⁰Heazlewood, B.R., Lewandowski, H.J. Chemistry Using Coulomb Crystals. ACS Symposium Series, vol. 1398, pp. 389–410. American Chemical Society, (2021)
- ³¹ Krohn, O.A., Catani, K.J., Lewandowski, H.J. Formation of astrochemically relevant molecular ions: Reaction of translationally cold CCl⁺ with benzene in a linear ion trap. Phys. Rev. A 105, 020801 (2022)

METHODS

A. Trap details and chirped excitation mass measurement

This experiment takes place in a linear Paul trap (Extended Data Fig. 1) mounted to a closed-cycle helium cryocooler,

which allows for both cryo-pumping and buffer gas tagging at cryogenic temperatures. Relevant trap parameters are listed in Extended Data Fig. 5. Oscillating RF voltages applied to two opposing rods create a stable trapping region along the radial (r) direction of the trap for particles with charge Q and mass m when the Matthieu parameter $q = \frac{2QV}{mr^2\Omega^2} < 0.9$. In practice, the trap is operated at $0.2 < q_{88} < 0.4$ in order to stably confine a wide range of masses. An oscillating voltage applied to a trap electrode at the mass-dependent radial secular frequency $\omega_r \approx \frac{QV}{\sqrt{2mr^2\Omega}}$ is used for mass-selective ejection of unwanted species from the trap, for example after a reactive collision with background gas.

The coupling between the ions along the axial (Z) direction of the trap, arising from their mutual Coulomb interaction, is strong compared to the static field (U_0) applied to the ring-shaped endcap electrodes. A two ion Coulomb crystal has two modes of oscillations along the axial direction: a center of mass ($\omega_{z,COM}$) and breathing ($\omega_{z,BM}$) mode. The oscillation frequencies of these modes depend on the mass of both ions, $\mu = m_{Sr}/m_{molecule}$ as shown in Eqn. (1), (2)^{32–34}. Both modes are observed, but $\omega_{z,COM}$ is easier to drive and detect as it does not require a field gradient to excite. Hence, it is the mode used for the non-destructive mass detection.

$$\omega_{z,COM}^2 = [(1+\mu) - \sqrt{1-\mu + \mu^2}]\omega_{z,88}^2 \tag{1}$$

$$\omega_{z,BM}^2 = [(1+\mu) + \sqrt{1-\mu+\mu^2}]\omega_{z,88}^2$$
 (2)

In a typical experimental cycle, a single ⁸⁸Sr⁺ is trapped and the secular frequency is measured to serve as a calibration. A single molecule is mass-selected before co-trapping with ⁸⁸Sr⁺, and the mass is verified by an additional secular frequency measurement. Although we use only two total ions for this spectrum, the number of ⁸⁸Sr⁺ cooling partners could easily be increased to improve the sympathetic cooling efficiency for the molecule. This may be advantageous for molecules with a large mass disparity compared to ⁸⁸Sr⁺, where the sympathetic cooling efficiency with a single cooling partner is poor.

We directly measure the axial secular frequency of molecule_88Sr⁺ pair through a chirped-ringdown measurement.¹⁹ "Chirp," here, refers to a pulsed cosine waveform whose frequency increases linearly in time over the duration of the pulse. Such a waveform in the time domain corresponds to an approximate square wave in the frequency domain. The chirp is tuned to sweep across the expected secular frequencies for a Coulomb crystal in our trap, and is applied to a trap endcap to drive axial motion. When the chirp frequency approaches the axial secular frequency of the ion pair, the ions oscillate in phase with a large amplitude. This oscillation Doppler shifts the ⁸⁸Sr⁺ ion in and out of resonance with the 422 nm cooling light, modulating its resulting fluorescence intensity at the ions' secular frequency. Though the chirp frequency quickly sweeps past the ions' secular frequency, they continue to oscillate with decaying

amplitude, producing a "ringdown" in the observed fluorescence modulation (Extended Data Fig. 2). This decay timescale is the result of damping caused by the $^{88}\mathrm{Sr}^+$ laser cooling process, and the strength of this damping depends on the 422 nm laser detuning and intensity relative to the 5p $^2\mathrm{P}_{1/2} \to 5\mathrm{s}\ ^2\mathrm{S}_{1/2}$ cooling transition. We typically operate 60 MHz red-detuned from resonance and slightly below the saturation intensity of the transition in order to maximize the modulated fluorescence signal.

The chirp amplitude applied to the trap has a typical amplitude on the order of 10 mV peak to peak, sweeping from 25 – 35 kHz over a span of 3 ms. A 2 ms ringdown time after the chirp allows the Doppler modulated fluorescence to decay as the ions cool back to equilibrium. This cycle is then repeated many times to allow for signal averaging. During the chirp cycle, fluorescence is collected by a PMT, the output of which is averaged on an oscilloscope triggered on the beginning of the chirp waveform. About 2000 averages of the fluorescence collected over the chirp cycle are required for a clear fluorescence modulation signal and typically takes about 30 s to acquire. The fluorescence signal is Fourier transformed to extract a secular frequency as shown in Extended Data Fig. 2 in order to verify the mass of the analyte molecule and the presence of the N₂ tag. Chirp parameters and number of averages are changed for other molecules with different expected secular frequencies and potentially slower sympathetic cooling rates in the case of a large size mismatch. Using this method, we observe masses ranging from about 50 - 260 Da.

B. Individual Molecule Data Sets

The spectrum plotted in fig. 3b) in the primary text is an average of eight different single molecule spectra as shown in Extended Data Fig. 3. Summing across all Tr⁺ molecules that were interrogated, a total of three de-tagging measurements were observed at every frequency step in the spectrum. More than one Tr⁺ was needed to acquire this full spectrum, as we suspect background O₂ periodically reacted with the molecules during investigation. The occasional formation of SrO⁺ indicates the presence of reactive background collisions. The spectral data from each of these eight molecules is plotted below in the order in which they were recorded.

We note that each time data taking commenced with a new Tr⁺ molecule we verified the presence of the strong transition near 3042 cm⁻¹ in order to confirm that it was a Tr⁺ rather than a Bz⁺ isomer. Additionally, we calibrate the frequency axis of our spectra using two different references. We record absorption spectra with our mid-IR source for solid polystyrene as well as ammonia vapor. Known peak positions for both species are provided by NIST, and we fit a simple linear calibration curve to this reference data and apply this linear transformation to our observed frequency data.

Each mid-IR frequency data point shows a distribution of de-tagging rates as shown in Extended Data Fig. 4. The full set of de-tagging data shown in Extended Data Fig. 3 was compiled into the spectrum reported in the primary text.

C. Computational details

Preliminary computational results indicate that there may be multiple energetically competitive attachment points for N_2 on Tr^+ . Two degenerate "face" sites have been identified, for which N_2 is orthogonal to the Tr^+ plane; and seven degenerate "side" sites, for which N_2 lays in the Tr^+ plane. As previously noted, we see strong experimental evidence that only one such tagging site is ever occupied during this experiment, implying that one of the above possibilities must be much more energetically favorable than the alternatives. The de-tagging spectrum which we observe is affected by the exact tagging site, however, as the various geometries have various levels of symmetry. Effort was therefore made computationally to distinguish the two classes of tagging sites in an effort to identify the tagging site which we observe experimentally.

Geometry optimization of the tagged structures was performed using several different methods: B3LYP-D3, M06-2X, and MP2, all using Dunning's aug-cc-pVTZ basis sets³⁵ in the Gaussian 16 software package³⁶. Results were, however, inconclusive (Extended Data Fig. 6), with DFT methods finding a higher binding energy for side tagged species, and MP2 methods finding higher binding energies for face tagged sites. Importantly, all of the calculated binding energies are well below the IR photon energies used in this work, so that all reported de-tagging events arise from single-photon processes. However, the inconclusive results suggest necessity of more expensive coupled cluster calculations for this system.

D. Notes on data analysis

We measure the mid-IR exposure time required for a detagging event, T, and model it as a random variable following an exponential distribution. Once a tagged molecule has absorbed a resonant photon, de-tagging occurs at the picosecond level. This time scale is much shorter than the time between individual pulses of our mid-IR pulsed laser, which has a repetition rate of 150 kHz. At a given mid-IR laser frequency, ω_L , the probability that a tagged molecule de-tags during a laser pulse is a constant. As a result, the probability that the de-tagging event happens right after a sequence of pulses is exponential in the number of pulses. Since the total exposure time before de-tagging is proportional to the total number of exposure pulses, T is an exponentially distributed random variable. The probability density function of the distribution is characterized by the wavelength-dependent exponential time constant $\tau(\omega_L)$, which can be expressed as

$$p(T, \omega_L) = \frac{1}{\tau(\omega_L)} e^{\frac{-T}{\tau(\omega_L)}}$$
(3)

Upon exposure to mid-IR light, de-tagging occurs on a timescale faster than the detection time for our mass measurement methods. In order to extract a meaningful rate, the mid-IR laser is gated via a mechanical shutter into a sequence of exposures. The 2.5 second intervals between exposures allow the lock-in signal to respond to the mass change to the

molecule caused by a de-tagging event. The first several of these exposures last for tens of milliseconds each, allowing us to capture fast de-tagging events. After a set number of constant fast exposures, the exposure duration is increased exponentially in order to observe slow de-tagging events within a reasonable experimental timescale.

When a de-tagging event is observed, the start time, T_s is defined as the total time the molecule was exposed to the mid-IR radiation before the final de-tagging pulse. The final time, T_f , is taken as T_s plus the length of the final pulse. The detagging event occurring sometime between these two T_s and T_f . Given the probability distribution 3, the probability of observing a de-tagging event between T_s and T_f is

$$P(T_s, T_f | \tau(\omega_L)) = e^{-\frac{T_s}{\tau(\omega_L)}} - e^{-\frac{T_f}{\tau(\omega_L)}}$$
(4)

For three independent measurements per point, this becomes

$$P(T_i|\tau(\omega_L)) = \prod_{i=1}^{3} \left[e^{-\frac{T_{s,i}}{\tau(\omega_L)}} - e^{-\frac{T_{f,i}}{\tau(\omega_L)}} \right]$$
 (5)

Assuming that the prior probability of $ln(\tau(\omega_L))$ is uniformly distributed, the maximum *a posteriori* estimation or the maximum likelihood estimation of the distribution parameter $\tau(\omega_L)$ is achieved by maximizing the likelihood function $L_3(\tau(\omega_L)|T_i) = P(T_i|\tau(\omega_L))$ with respect to $\tau(\omega_L)$. We maximize this function numerically to determine this most likely value for $\tau(\omega_L)$. We also determine a 95% confidence level numerically based on the distribution of the likelihood functions. The density of the confidence level is proportional to the posterior probability density, and we have

$$CL(CI_{min} < \tau < CI_{max}) \equiv \frac{\int_{\tau = CI_{min}}^{\tau = CI_{max}} L_3(\tau | T_i) dln(\tau)}{\int_{\tau = 0}^{\tau = +\infty} L_3(\tau | T_i) dln(\tau)}$$
(6)

We choose the interval where the likelihood function $L_3(\tau(\omega_L)|T_i) > e^{-2} \cdot L_{3,max}$ as our confidence interval, and verify that this corresponds to a confidence level of $\gtrsim 95\%$.

From the point of view of random sampling, our method of data analysis can be well justified when ignoring the slight broadening and distortion of the likelihood function due to the uncertainty caused by the finite exposure time from our shuttered laser source. Assuming the observations T_i constitute N random samples subjected to an exponential distribution with the time constant τ_0 , and $dT_i \equiv T_{f,i} - T_{s,i} \ll \tau_0$ for all i, we have,

$$L_N(\tau|T_i) = \prod_{i=1}^N \left[\frac{dT_i}{\tau} e^{-\frac{T_i}{\tau}} \right] \tag{7}$$

The likelihood function is maximum when $\tau = \frac{\sum_{i=1}^{N} T_i}{N}$, which gives an unbiased estimator of τ_0 . Notably, the likelihood function L_N can be normalized by a factor $(\frac{\sum_{i=1}^{N} T_i}{N})^N$.

 $\frac{1}{\prod_{i=1}^N dT_i}$ to give a function only of the number of samples N and the relative magnitude of τ and $\frac{\sum_{i=1}^N T_i}{N}$. This indicates that for a given N, L_N is always proportional to a fixed function $ln(\frac{N\tau}{\sum_{i=1}^N T_i})$. This differs from cases where random variables are normally distributed. For any v>u>0, if we choose the confidence interval to be $CI=(u\cdot\frac{\Sigma T_i}{N},v\cdot\frac{\Sigma T_i}{N})$, the confidence level is a constant for any set of T_i and equal to

$$CL(u \cdot \frac{\sum T_i}{N} < \tau < v \cdot \frac{\sum T_i}{N}) \equiv \frac{\int_{\tau = CI_{min}}^{\tau = CI_{max}} L_N(\tau | T_i) dln(\tau)}{\int_{\tau = 0}^{\tau = +\infty} L_N(\tau | T_i) dln(\tau)}$$
$$= P(\frac{\tau'}{v} < \frac{\sum T_i'}{N} < \frac{\tau'}{u} | \tau') \quad (8)$$

The right-hand side of Eqn. 8 is the probability that the arithmetic mean of N random samples from an exponential distribution with time constant τ' falls within the interval $(\frac{\tau'}{\nu},\frac{\tau'}{u})$. It is a constant for any $\tau'>0$. If we consider a special case where $\tau'=\tau_0$, the right-hand side of Eqn. 8 is also the probability that the confidence interval determined for N samples includes the true value τ_0 . Hence, our method gives a reasonable estimation of the time constant, confidence interval and the confidence level.

Two wavelengths were chosen to test this model of the distribution, with a sample histogram at 2950 cm $^{-1}$ shown in Fig. 4 of the Extended Data. For this test, we measured 20 detagging times for ${\rm Tr}^+$ irradiated with single frequency laser light at 2950 cm $^{-1}$. We observe a uniform distribution which is consistent with the exponential model described above. Additionally, we see no evidence of bimodality in this distribution, which might arise if the ${\rm N}_2$ attaches to ${\rm Tr}^+$ at different sites during successive measurements. Such effects from multiple tagging sites could be readily observed in other systems, however, by measuring the de-tagging time distribution for observed transitions at a single laser frequency.

II. DATA AVAILABILITY

All data taken is presented. Raw data are available from the corresponding author on request.

III. ADDITIONAL REFERENCES

³²Kielpinski, D., et al. Sympathetic cooling of trapped ions for quantum logic. Phys. Rev. A 61, 032310 (2000)

³³Rajagopal, V., Marler, J.P., Kokish, M.G., Odom, B.C. Trapped ion chain thermometry and mass spectrometry through imaging. Eur. J. Mass Spectrom. 22(1), 1–7 (2016)

³⁴Fan, M., et al. Optical mass spectrometry of cold RaOH⁺ and RaOCH₃⁺. Phys. Rev. Lett. **126**, 023002 (2021)

³⁵Dunning Jr., T.H. Gaussian basis sets for use in correlated molecular calculations. i. the atoms boron through neon and hydrogen. J. Chem. Phys. 90(2), 1007–1023 (1989)

³⁶Frisch, M.J., et al. Gaussian~16 Revision C.01. Gaussian Inc. Wallingford CT (2016)

IV. ACKNOWLEDGMENTS

This work has been supported by the US National Science Foundation (NSF PHY-1912105) and the Air Force Office of Scientific Research (MURI FA9550-20-1-0323). We thank Mark Johnson and his group for many useful discussions.

V. AUTHOR CONTRIBUTIONS

A.C., S.E., and Z.P. designed the experiment, built the apparatus, and took the data. All three contributed equally to this work. M.B. designed and built peripheral systems. L.S. provided computational support. D.P. oversaw the effort.

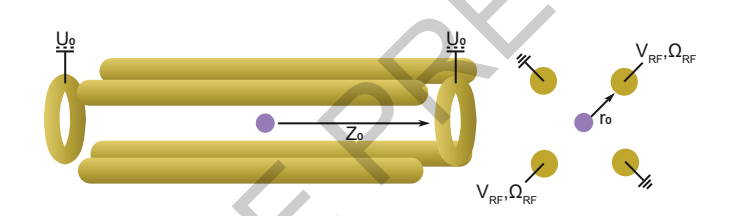
VI. COMPETING INTERESTS

The authors declare no competing interests.

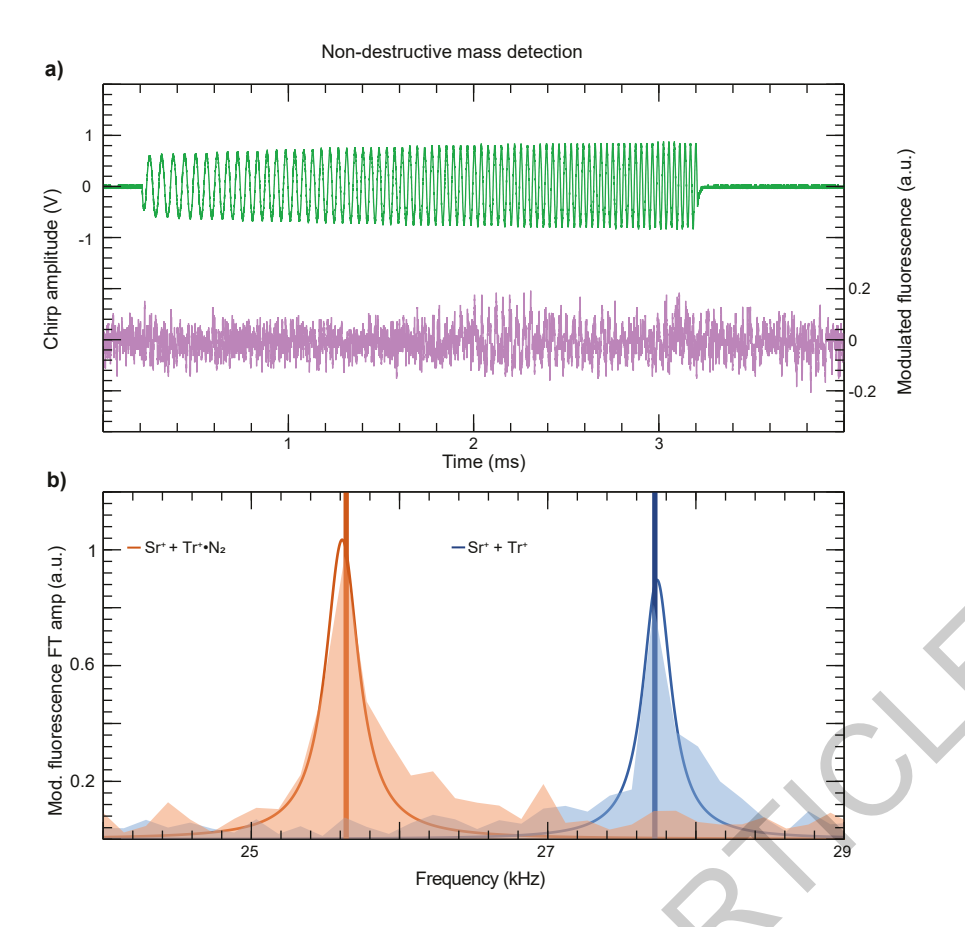
VII. ADDITIONAL INFORMATION

A Methods section describing the experimental setup and data analysis in more detail is available for this paper. Reprints and permissions information available at www.nature.com/reprints. Correspondence and requests for materials should be addressed to D.P. (davepatterson@ucsb.edu).

VIII. EXTENDED DATA

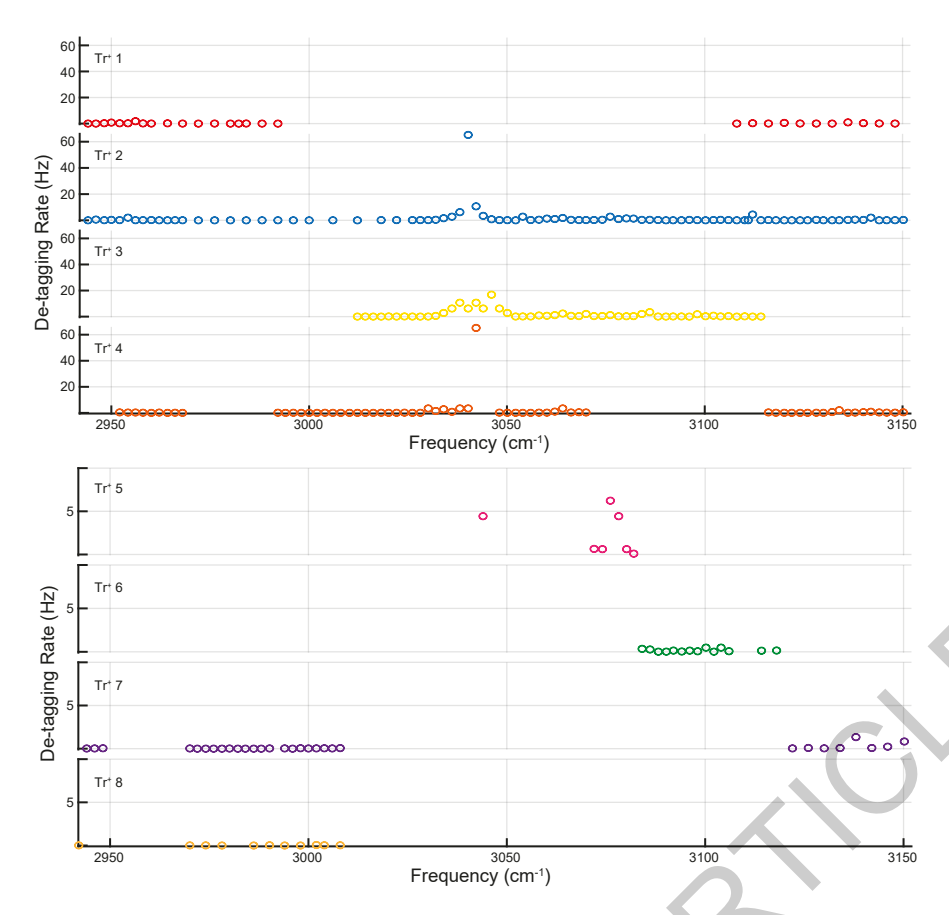


Extended Data Figure 1: Trap diagram | A sketch of the trap showing the side view (left) and cross sectional view (right) for relevant parameters described in Extended Data Figure 5.



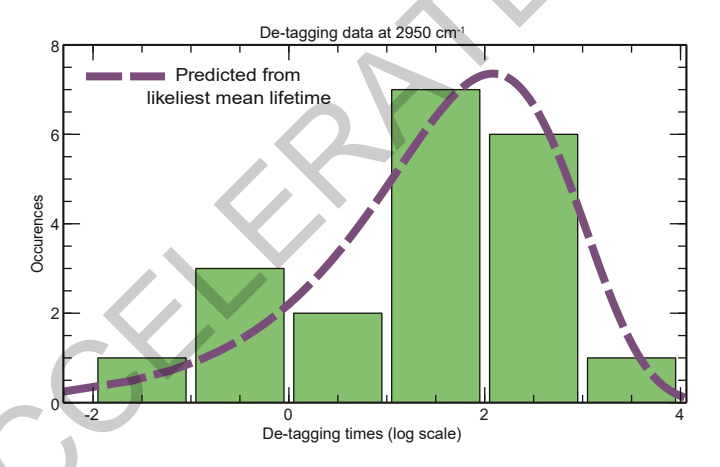
Extended Data Figure 2: Non-destructive mass detection

a) An example chirp waveform applied to the ion pair (green) and the resulting modulated fluorescence (purple). Ion oscillation can be seen to begin around the 2 ms point. b) The modulated fluorescence signal is Fourier transformed (shaded) and fit with a Lorentzian function (line profile) to extract a center frequency used for mass determination. Vertical bars indicate the calculated secular frequency from the measured single ⁸⁸Sr⁺ secular frequency (not shown).



Extended Data Figure 3: Individual molecular spectra

The data points recorded for each of the eight individual molecules used in the averaged spectrum in the main text. The majority of points in the spectrum were recorded with the first four molecules, and the remainder were used primarily to observe background points.



Extended Data Figure 4: Single mid-IR frequency de-tagging histogram | A sample histogram of 20 lifetime measurements on the weak spectral feature at 2950 cm⁻¹ shows consistency with the model of the exponential distribution.

Trap parameter	value	unit
Q	+e	С
V	40 - 70	V
m	50 - 260	Da
r	2	mm
Ω	$2\pi \times 1.6$	MHz
z_0	8.4	mm
U_0	50	V
$\omega_{r,88}$	$2\pi \times 90 - 270$	kHz
$\omega_{r,88}$ $\omega_{z,88}$	$2\pi \times 28$	kHz

Extended Data Figure 5: Trap parameters | Typical trap parameters for our cryogenic linear Paul trap used in this experiment. Figure 1 in the Extended Data displays a trap diagram.

Method	race Lb (IX)	race Eb (cm)	Dide EP (IX)	Side D6 (cm	-)
B3LYP-D3	948.7	659.4	889.1	617.9	
MP2	1313.3	912	1143.6	794	
M06-2X	679.4	472	713.8	496	
		y			

Extended Data Figure 6: Computational results \mid A table of computed binding energies in K and cm⁻¹.